Geomechanics and Engineering, *Vol. 19, No. 3 (2019) 217-227*
DOI: https://doi.org/10.12989/gae.2019.19.3.217

An improved model of compaction grouting considering three-dimensional shearing failure and its engineering application

Liang Li[a], Zhou-Chen Xiang[b], Jin-Feng Zou* and Feng Wang[c]

School of Civil Engineering, Central South University, No.22, Shaoshan South Road, Central South University Railway Campus, Changsha, Hunan Province, People's Republic of China

(Received November 22, 2018, Revised September 3, 2019, Accepted October 14, 2019)

Abstract. This study focuses on an improved prediction model to determine the limiting grouting pressure of compaction grouting considering the ground surface upheaval, which is caused by the three-dimensional conical shearing failure. The 2D-dimensional failure curve in Zou and Xia (2016) was improved to a three-dimensional conical shearing failure for compaction grouting through coordinate rotation. The process of compaction grouting was considered as the cavity expansion in infinite Mohr-Coulomb (M-C) soil mass. The prediction model of limiting grouting pressure of compaction grouting was proposed with limit equilibrium principle, which was validated by comparing the results in El-Kelesh *et al.* (2001) and numerical method. Furthermore, using the proposed prediction model, the vertical and horizontal grouting tube techniques were adopted to deal with the subgrade settlement in Shao-huai highway at Hunan Provence of China. The engineering applicability and effectiveness of the proposed model were verified by the field test. The research on the prediction model for the limiting grouting pressure of compaction grouting provides practical example to the rapid treatment technology of subgrade settlement.

Keywords: compaction grouting; limiting grouting pressure; cavity expansion; three-dimensional conical shearing failure; subgrade settlement treatment

1. Introduction

Compaction grouting technique has been widely used to enforce soft foundation, surrounding rock, tunnel face, pile, correction of building, subgrade subsidence, etc. (Chen *et al.* 2015, Ibrahim *et al.* 2015, Zhang *et al.* 2015, Pan *et al.* 2017, Ukritchon *et al.* 2017, Pan *et al.* 2018, Zou *et al.* 2018, Zou *et al.* 2019a, Chen *et al.* 2019a, Zou *et al.* 2019b, Zou and Zhang 2019, Chen *et al.* 2019b, Chen *et al.* 2019c). The Theoretical basis of compaction grouting is cavity expansion theory, which has been widely developed and applied to modeling complex geotechnical problems, such as determination of foundation bearing capacity, grouting, stability analysis of surrounding rock and soil characterizations based on pressuermeter tests etc. (Vesic 1972, Carter *et al.* 1986, 2010, Wang *et al.* 2012, Chai *et al.* 2014, Fahimifar *et al.* 2015, Yang and Yan 2015, Yang and Pan 2015 , Xiao *et al.* 2015, 2017, Zhou *et al.* 2015, 2016, Zou *et al.* 2016, Zou and Xia 2017, Zou and Wei 2018, Zou *et al.* 2019c, Li *et al.* 2019). In most instances, the problem has been simplified to spherical or cylindrical cavity expansion in a homogeneous and isotropic soil mass of infinite extent. Although many of analytical and numerical solutions for compaction grouting pressure based on cavity expansion theory have been proposed to solve practical engineering problems (Brown and Warner 1973, Warner and Brown 1974, Wang *et al.* 2010, 2013, El-Kelesh *et al.* 2012, Fischer *et al.* 2012, Yea *et al.* 2013, D'Antonio *et al.* 2014, Taylor and Choquet 2012, Pegues *et al.* 2015, Szynakiewicz 2016), few of literatures focused on the grouting pressure, which leads the ground surface upheaval caused by the conical shearing failure. For example, Graf (1969) indicated that if the grout material is injected into the holes under continuous pressure, the compaction of the soil mass surrounding the grout bulb will increase to a maximum and then the pressure will cause a conical shearing of the soil mass above the grout bulb. Therefore, the upward force is governed by the weight of the cone of soil above the grout bulb, as well as by the downward shearing resistance. Based on Graf's findings and the Mohr-Coulomb criterion, Wong (1971, 1974) developed a simplified analytical model for the failure of soil mass caused by compaction grouting, which is usually used to estimate the limiting grouting pressure. El-Kelesh *et al.* (2001) proposed a theoretical model that describes the mechanics of the compaction grouting process and rationally considers the different soil and grouting parameters, which governs the overall design and performance of the method. This model, coupled with Wong's model, can be used to determine the limiting grouting pressure. Hossain and Yin (2014) studied the behavior of the pressure-grouted soil-cement interface and the shear strength of the soil-cement grout interface of soil

*Corresponding author, Professor
E-mail: zoujinfeng_csu@163.com
[a]Professor
E-mail: liliang_csu@126.com
[b]Master Student
E-mail: 370033475@qq.com
[c]Ph.D. Student
E-mail: wangfeng687@126.com

ISSN: 2005-307X (Print), 2092-6219 (Online)

nailing via direct shear tests. However, the presented results could not consider the conical shearing failure in three-dimensional space.

The main objective of this study is to introduce an improved prediction model for the limiting grouting pressure of compaction grouting based on the three-dimensional conical shearing failure and cavity expansion theory in M-C soil mass. In addition, the proposed model is used to guide the subgrade settlement treatment of the Shao-huai K1302 highway.

2. Theoretical model

2.1 Expansion of grout bulb

In this study, the compaction grout bulb is modeled as a spherical cavity expansion in an isotropic elastic-plastic continuum as shown in Fig. 1.

It is assumed that a grout bulb is injected into ground after drilling without disturbing the surrounding soil mass, which firmly seals the grout pipe to surrounding ground. At the beginning of injection, the radius of grout bulb is drilling radius Ri and soil mass has an isotropic effective stress q. The grout bulb radius will expand to R and the plastic state will appear in a spherical zone with radius R_p around bulb when a uniformly distributed internal pressure at grout-soil interface is increased to p. Beyond the elastoplastic interface, the soil mass remains in a state of elastic equilibrium. Meanwhile, it can be assumed that any variation in stress due to body force is negligible when compared with the existing and newly applied stresses. Hence, the condition of spherical symmetry holds for the expansion process and the behavior can be described in terms of spherical polar coordinates (r,θ,ω). It follows from the symmetry that all the shear components of stress vanish (σ_ω=σ_θ) and the equilibrium equation of an element in plastic zone (Fig.1), at distance from the center, is given by,

$$\frac{\partial \sigma_r}{\partial r} + 2\frac{\sigma_r - \sigma_\theta}{r} = 0 \tag{1}$$

where, σ_r and σ_θ are radial stress and circumferential stresses, respectively.

The yield condition, according to the Mohr-Coulomb criterion, is represented as,

$$\sigma_r + c\cdot\cot\varphi = N\left(\sigma_\theta + c\cdot\cot\varphi\right) \tag{2}$$

where, $N = \dfrac{1+\sin\varphi}{1-\sin\varphi}$.

Boundary conditions is

$$\sigma_r = p \quad \text{for} \quad r = R \tag{3}$$

According to the volume conservation law, the total volume change of spherical cavity expansion is equal to those in elastic and plastic zones, which can be expressed as follows (Vesic 1972).

$$R^3 - R_i^3 = {R_p}^3 - \left(R_p - u_p\right)^3 + \left({R_p}^3 - R^3\right)\Delta \tag{4}$$

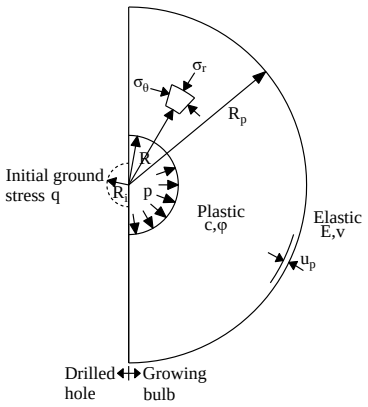

Fig. 1 Growth of grout bulb

where, R_i is the original radius of grouting bulb; R_p is the final radius of grouting bulb; and Δ is the average volumetric strain in plastic region; up is the radial displacement of elastic-plastic interface which can be calculated from Lamé's solution as follows

$$u_p = \frac{1+v}{2E} R_p\left(\sigma_p - q\right) \tag{5}$$

where, σ_r=σ_p for r=R_p.

Combining Eqs. (1)-(2), and considering boundary condition in Eq. (3), the following solution is obtained

$$\sigma_r = \left(p + c\cdot\cot\varphi\right)\left(\frac{R}{r}\right)^{\frac{4\sin\varphi}{1+\sin\varphi}} - c\cdot\cot\varphi \tag{6}$$

Hence, stress σ_p could be given by

$$\sigma_p = \left(p + c\cdot\cot\varphi\right)\left(\frac{R}{R_p}\right)^{\frac{4\sin\varphi}{1+\sin\varphi}} - c\cdot\cot\varphi \tag{7}$$

At the junction of the elastic and plastic zone, just for r= R_p, the stress σ_r and σ_θ must satisfy the limit equilibrium principle.

$$\left(p + c\cdot\cot\varphi\right)\left(\frac{R}{R_p}\right)^{\frac{4\sin\varphi}{1+\sin\varphi}} = \frac{3\left(q + c\cdot\cot\varphi\right)\left(1+\sin\varphi\right)}{3-\sin\varphi} \tag{8}$$

Combining Eqs. (4), (5), (7) and (8), and neglecting the higher upward force as well as R^3, the following expression for R_p is obtained.

$$\left(\frac{R_p}{R}\right)^3\left[\frac{2\left(1+v\right)\left(c+q\cdot\tan\varphi\right)}{E} + \Delta\right] = 1+\Delta \tag{9}$$

where, I_r is the rigidity index and I_{rr} is reduced rigidity index.

$$I_r = \frac{E}{2\left(1+v\right)\left(c+q\cdot\tan\varphi\right)} \tag{10}$$

$$I_{rr} = \frac{I_r}{1+I_r\Delta} \tag{11}$$

where, q is the initial stress of soil, q=$k_0\cdot\gamma\cdot$L, in which k_0 is the lateral pressure coefficient and k_0=1-sinφ

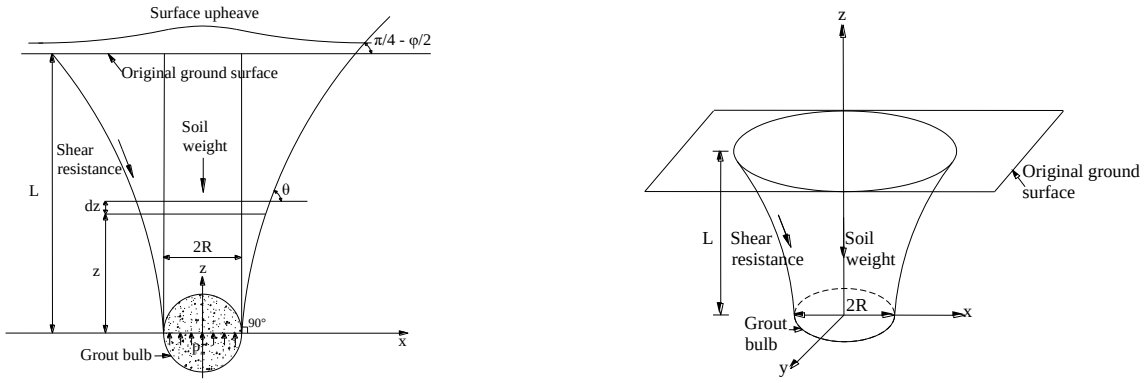

Fig. 2 Growth of grout bulb

Then, substituting Eqs. (10)-(11) into Eq. (9), the following expression for R_p is simplified by

$$\frac{R_p}{R}=\sqrt[3]{I_{rr}} \tag{12}$$

2.2 Three-dimensional conical shearing failure

When grouting pressure exceeds a certain value or the grouting time exceeds a certain value, there will be upward movement in the upper soil mass. It is reasonable to assume that it is the upward force (T) exerted by grouting pressure which overcomes the total downward force (G), resulting from the weight of cone of soil mass above the grout bulb, and the downward shearing resistance (F) along the cone surface. In this study, the 2D-dimensional failure curve in Zou and Xia (2016) was adopted and improved to three-dimensional conical shearing failure for compaction grouting through coordinate rotation, as shown in Fig.2.

Based on the improved model, considering the ground surface upheaval, the limiting grouting pressure can be determined. The curve equation of failure surface for the grouted soil mass can be expressed as (Zou and Xia 2016)

$$x(z)=R+\frac{L}{(n+1)\tan(\pi/4-\varphi/2)}\left(\frac{z}{L}\right)^{(n+1)} \tag{13}$$

where, φ is the angle of internal friction; L is the grouting depth; n is parameter of failure surface shape ($0< n <1$).

In Fig.2, the conical surface is inclined by an angle $\pi/4$-$\varphi/2$ to the horizontal, which is equivalent to the application of the Mohr-Coulomb failure criterion. This model could be given by

$$T \geq G+F \tag{14}$$

where, T, G and F are given by

$$T=\pi R^2 p_u \tag{15}$$

$$G=\gamma V \tag{16}$$

$$F=Q\cdot\sin\theta=C_u S\cdot\sin\theta \tag{17}$$

where, θ is the angle between the conical surface and horizontal; R is the radius of the spherical grouted; p_u is the grouting pressure; γ is the unit weight of the soil; V is the volume of the grouted soil; C_u is the undrained resistance of soil and S is the lateral area of the grouted soil.

The equilibrium of the rotating surface volume requires that,

$$dV=\pi x(z)^2\,dz \tag{18}$$

Eq. (18) can be solved by integrating from 0 to L, and the volume of grouted soil mass above the grout bulb can be expressed as

$$V=L\pi\left[\frac{L^2}{(n+1)^2(2n+3)\tan^2(\pi/4-\varphi/2)}+\frac{2LR}{(n^2+3n+2)\tan(\pi/4-\varphi/2)}+R^2\right] \tag{19}$$

According to the shear resistance equilibrium of infinitesimal element, dF can be obtained as follows

$$dF=C_u dS\cdot\sin\theta=C_u\cdot 2\pi x(z)\frac{dz}{\sin\theta}\cdot\sin\theta \tag{20}$$

Eq. (20) can be solved by similar approach and expressed as

$$F=2\pi L\left[\frac{L}{(n^2+3n+2)\tan(\pi/4-\varphi/2)}+R\right] \tag{21}$$

Combining Eqs. (14), (19) and (21), a relationship between grout bulb radius R and grouting pressure p_u, which satisfies the ground surface upheaval, could be obtained as follows

$$p_u=\frac{\gamma L}{R^2}\left[\frac{L^2}{(n+1)^2(2n+3)\tan^2(\pi/4-\varphi/2)}+\frac{2RL}{(n^2+3n+2)\tan(\pi/4-\varphi/2)}+R^2\right]+\frac{2LC_u}{R^2}\left(\frac{L}{(n^2+3n+2)\tan(\pi/4-\varphi/2)}+R\right) \tag{22}$$

It can be seen from Eq. (22) that the grouting pressure required for ground surface upheaval is related to unit weight of soil γ, grouting depth L, grout bulb radius R and undrained resistance of soil C_u. Furthermore, the grouting depth has great influence on the grouting pressure.

3. Limiting grouting pressure

In process of the compaction grouting technique, it is assumed that the injection process continues until a limiting

condition is reached. In many engineering practices, ground surface upheaval is the limiting condition. The upward force exerted by the grouting pressure, which is controlled by the model from Eq. (22), causes conical shearing failure and upward movement of soil mass above the grout bulb, which lead to some ground surface upheaval. However, the stage of spherical cavity expansion will be happened before ground surface upheaval. At a certain depth, the bulb radius will increase with the grouting pressure within a certain range during injection, causing ground surface upheaval. Therefore, it is possible to develop a relationship governing the applied pressure and the corresponding bulb radius during injection, as follows.

Inserting Eq. (12) into Eq. (8), the pressure p is obtained in the following expression.

$$p = \frac{3(1+\sin\varphi)}{3-\sin\varphi}\left(q + c\cdot\cot\varphi\right)\left(I_{rr}\right)^{\frac{4\sin\varphi}{1+\sin\varphi}} - c\cdot\cot\varphi \tag{23}$$

Substituting Eqs. (12), (23) into Eq. (7), the following expression for σp can be obtained.

$$\sigma_p = \frac{3(1+\sin\varphi)}{3-\sin\varphi}\left(q + c\cdot\cot\varphi\right) - c\cdot\cot\varphi \tag{24}$$

Then inserting the expression for σ_p given by Eq. (24) into Eq. (5), u_p/R_p can be obtained as follows

$$\frac{u_p}{R_p} = \frac{1+\nu}{2E}\left(\frac{4\sin\varphi}{3-\sin\varphi}\right)\left(q + c\cdot\cot\varphi\right) \tag{25}$$

From Eq. (11), the average volumetric strain Δ can be given by the following expression

$$\Delta = \frac{1}{I_{rr}} - \frac{1}{I_r} \tag{26}$$

By dividing Eq. (4) by R^3, the following expression is obtained

$$\left(\frac{R_i}{R}\right)^3 = \left(\frac{R_p}{R}\right)^3\left[-1+\left(1-\frac{u_p}{R_p}\right)^3 - \left(1-\frac{R^3}{R_p^3}\right)\Delta\right] + 1 \tag{27}$$

Substituting Eqs. (12), (25), (26) into Eq. (27), the expression for R_i/R is obtained as follows

$$\left(\frac{R_i}{R}\right)^3 = a_1 I_{rr} + \frac{1}{I_{rr}} - \frac{1}{I_r} \tag{28}$$

in which

$$a_1 = \frac{1}{I_r} - 1 + \left(1 - \frac{1+\nu}{2E}\frac{4\sin\varphi}{3-\sin\varphi}\left(q + c\cdot\cot\varphi\right)\right)^3 \tag{29}$$

From Eq. (23), the reduced rigidity index I_{rr} can be expressed as a function of the pressure p as follows

$$I_{rr} = \left(\frac{p+a_2}{a_3}\right)^{a_4} \tag{30}$$

in which a_2, a_3, and a_4 are given by

$$a_2 = c\cdot\cot\varphi \tag{31}$$

$$a_3 = \frac{3(1+\sin\varphi)}{3-\sin\varphi}\left(q + c\cdot\cot\varphi\right) \tag{32}$$

$$a_4 = \frac{3(1+\sin\varphi)}{4\sin\varphi} \tag{33}$$

Combining Eqs. (28) and (30), the ratio R_i/R can be expressed as a function of the pressure p as follows

$$\left(\frac{R_i}{R}\right)^3 = a_1\left(\frac{p+a_2}{a_3}\right)^{a_4} + \left(\frac{a_3}{p+a_2}\right)^{a_4} - a_5 \tag{34}$$

in which, a_5 is given by

$$a_5 = \frac{1}{I_r} \tag{35}$$

Eq. (34) can also be rewritten as follows

$$R = R_i \Bigg/ \left[a_1\left(\frac{p+a_2}{a_3}\right)^{a_4} + \left(\frac{a_3}{p+a_2}\right)^{a_4} - a_5\right]^{\frac{1}{3}} \tag{36}$$

where, p is the applied pressure at the grout-soil interface; R is the grout bulb radius corresponding to the applied pressure p; R_i is the drilling radius; a_1, a_2, a_3, a_4 and a_5 are constants depending on the soil type.

Based on the spherical cavity expansion model given by Eq. (36) and the three-dimensional conical shearing failure model given by Eq. (22), limiting grouting pressure can be predicted. As shown in Fig. 4, the spherical cavity expansion model indicates that the bulb radius increases smoothly with the applied pressure until reaching a certain value, which also satisfies the conical shearing failure model (intersection point of the two curves). This pressure value is defined as the upward pressure p_{uph} at which the ground surface upheaval starts to occur. It also can be seen that, in the last portion of the injection curve, the bulb radius increases extremely sharply and tends to infinity as the pressure asymptotically approaches an ultimate value p_{ult}. Meanwhile, it is assumed that, before the excessive plastic deformation, the surrounding soil mass is in a plastic state. The pressure value associated with excessive plastic deformation $p_{ex\text{-}df}$ can be correlated with the ultimate pressure p_{ult}.

$$p_{ex-df} = \alpha\, p_{ult} \tag{37}$$

where, α is dimensionless failure factor ($\alpha<1.0$).

Therefore, the limiting grouting pressure p_{lim} at the grout-soil interface will be governed by p_{uph} or $p_{ex\text{-}df}$, whichever is smaller.

The grout hole spacing S_p can be expressed as

$$S_p = 2R_p \tag{38}$$

where, plastic radius R_p can be obtained by Eq. (12); R is the bulb radius corresponding to the limiting grouting pressure p_{lim}. According to the engineering experience, when the average volumetric strain of plastic zone is $\Delta>10^{-2}$, the soil structure will be destroyed. Hence, the average volumetric strain Δ is 0.01 in this study.

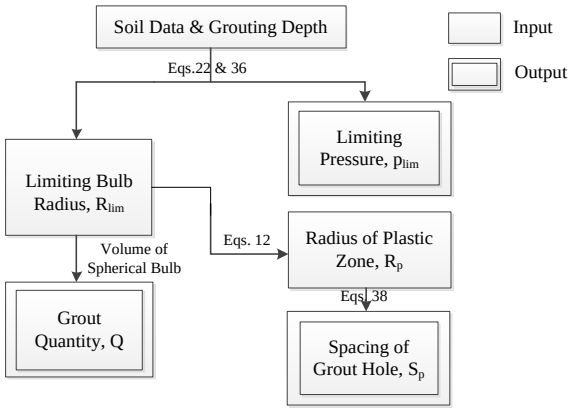

Fig. 3 Proposed compaction grouting model

Table 1 Properties of loose Chattahoochee River sand used in model validation

Soil	Initial void ratio, e_0	Angle of internal friction, φ	Modulus of deformation, E(kPa)
B-4	0.96	34.6	981,645
B-5	0.99	32.3	1,107,170
B-6	0.99	32.9	359,904

Note: Mean particle size = 0.37 mm; Coefficient of uniformity = 2.5;Specific gravity = 2.66; e_{max}= 1.10; e_{min} = 0.61

4. Methodology

Fig. 3 summarizes the computational procedure followed by the proposed compaction grouting model. The model inputs are the soil data and the grouting depth. The outputs to the model are the limiting pressure p_{lim}, maximum spacing of grout hole S_p and quantity of grout material Q.

5. Validations

5.1 Validations by published solutions

To verify the validity and effectiveness of the proposed model, the results of it are compared with the results in El-Kelesh *et al.* (2001). The derived formulations are programmed into a computer code, and sets of rock or soil mass parameters are adopted from El-Kelesh *et al.* (2001) as Table 1.

The results of the proposed approach and those of El-Kelesh's solution (2001) are presented in Fig.4 for n=0.5. In addition, the results of the proposed approach are compared with the reported actual data. The results for the predicted limiting pressures under different grouting depths (respectively, 2, 4 and 6 m) are shown in Fig.5.

It can be seen from Fig.4 that the results of the proposed approach are agreeable well with those of El-Kelesh *et al.* (2001), and the difference of the upward pressure p_{uph} is no more than 5%. The lower and upper limits of the reported actual pressures are 350 and 3500 kPa, respectively. As seen in Fig.5, all the predicted limiting pressures are within the range of the reported real ones.

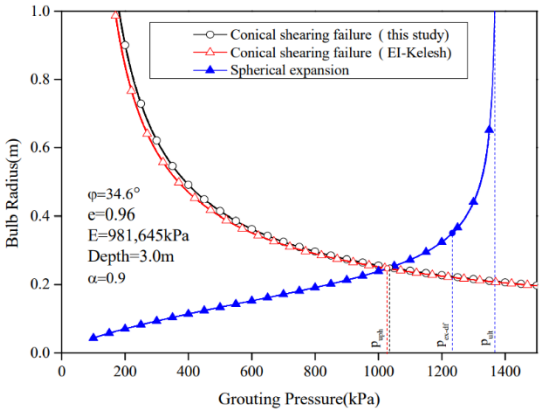

Fig. 4 Growth of grout bulb with injection until reaching limiting pressure

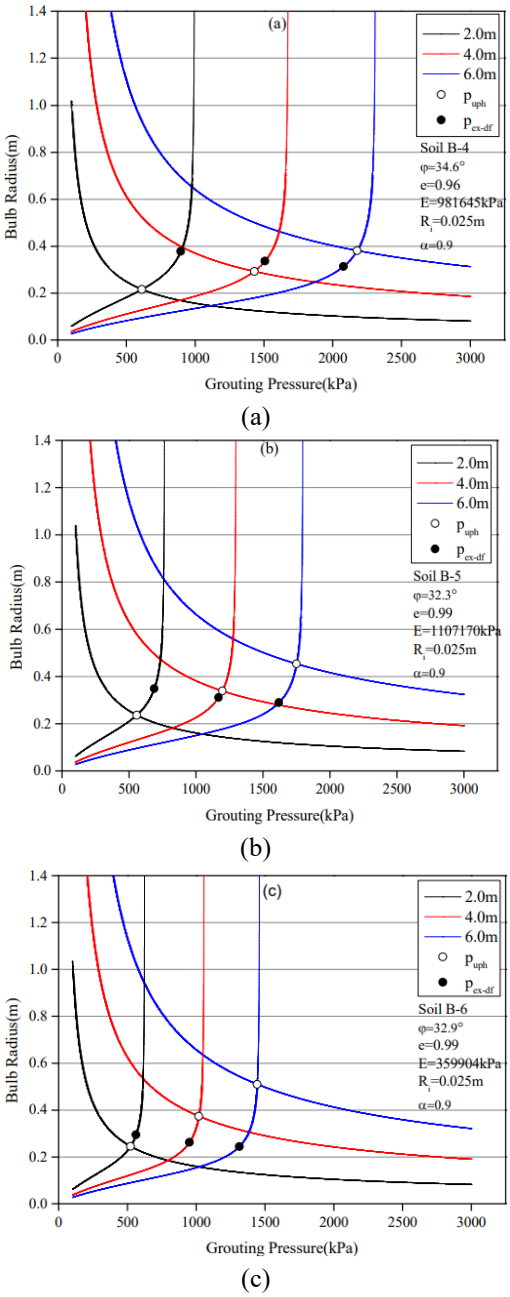

Fig. 5 Predicted limiting pressures at depths of 2.0, 4.0, and 6.0 m: (a) Soil B-4, (b) Soil B-5 and (c) Soil B-6

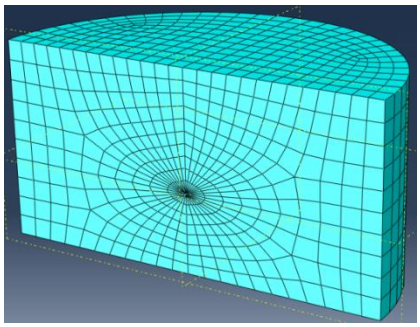

(a) Section plan

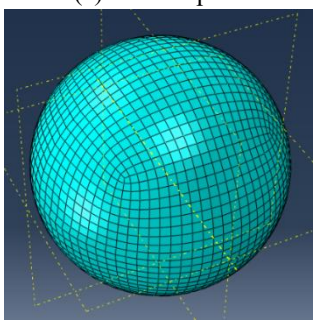

(b) Grout bulb

Fig. 6 Numerical grouting model and finite element mesh

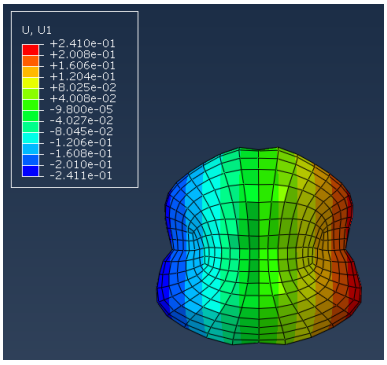

Fig. 7 Growth of grout bulb when h=3 m

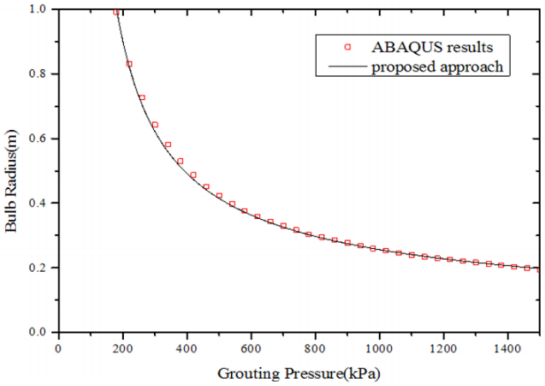

Fig. 8 Results of proposed solution and ABAQUS for the grouting pressure

5.2 Validations by numerical method

This section presents the results of the ABAQUS software to validate the proposed approach. In this numerical analysis, the soil is simplifies to a cylinder with radius of 5m and a height of 5m, where the center of the cylinder is a spherical grout bulb with radius of 0.025m and the distance from the ground surface to the bulb is 3m. The parameters of the numerical and theoretical calculations are selected from the study of El-Kelesh *et al.* (2001) as follows: E=981645kPa, v=0.3, γ=19.6kN/m^3, φ=34.6° and e=0.96. On the internal surface of the bulb, a uniform pressure p of 1000kPa is set to simulate the grout injection. Furthermore, the soil mass is modeled by the generalized M-C model. The result, grouting pressure, can be got from internal surface of soil.

Fig. 6 shows the finite element mesh of the compaction grouting model. The global seeds size of soil is set as 0.35m. The local seeds size of soil is set as 0.001m in the inner surface, as well as the spherical grout bulb. And the F.E. model is made of 13576 linear hexahedral elements of type C3D8R. Fig. 7 shows the growth of grout bulb under the injection pressure and extrusion of surrounding soil and Fig. 8 shows the results comparison of the proposed model and the numerical model.

It can be seen from Figs.7-8 that the results of the proposed approach are agreeable well with those of ABAQUS for the grouting pressure considering the ground surface upheaval.

6. Engineering application

To validate the proposed approach in engineering practice, the prediction model for the limiting grouting pressure is adopted to guide the design of the subgrade settlement treatment in Shao-huai highway Hunan province of China.

6.1 Engineering overview

According to the field geological data, the stratum of the subgrade settlement area of Shao-huai highway is simple, as shown in Fig. 9. Therefore, in order to simplify calculations, it can be assumed that the entire subgrade can be approximated as a single layer. The main mechanical parameters of each soil layer are obtained in laboratory test with on-site samples, and the parameters in Table 2 are the average values of the mechanical parameters of each layer. These parameters can be substituted into the proposed model to get the curve of the bubble radius R varying with the grouting pressure p. Based on this curve, parameters such as grouting depth, grouting pressure and grouting spacing when compaction grouting to reinforce the subgrade can be determined.

The right-subgrade of Shao-huai K1302 highway is in soft soil area, where bearing strength of the foundation

Table 2 The main mechanical parameters of each soil layer

Geotechnical name	Bottom elevation	Soil parameters (Average)
Filled soil	-7.6 ~ -3.4m	γ=15kN/m^3, E=8.5Mpa φ=15°, c=40kPa v=0.3, C_u=15kPa
Silty clay	-8.9 ~ -7.2m	
Silt	-13.6 ~ -8m	
Strong weathered limestone	-16.8 ~ -15.9m	

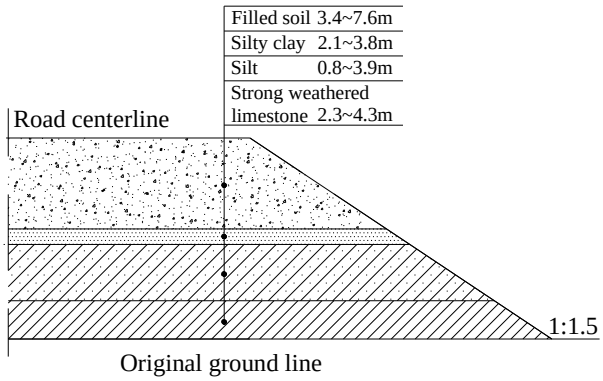

Fig. 9 Soil distribution

Fig. 10 Uneven settlement and pavement crack of Shaohuai highway

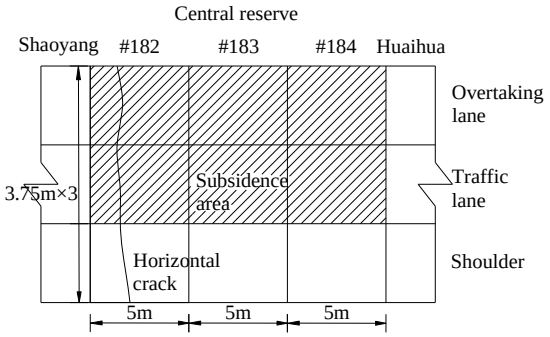

Fig. 11 Settlement area

is low and the groundwater level is high. Under the combined effect of the weight of subgrade soil mass, traffic load and groundwater, the uneven settlement and the pavement crack had been happened, where the maximum differential settlement have been increased to 12 cm in two months, as shown in Fig.10. The engineering properties of

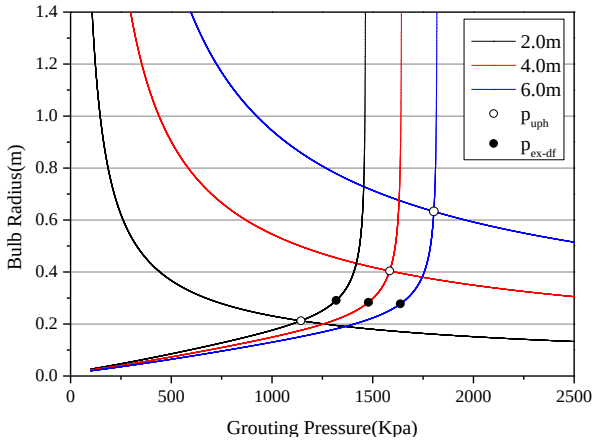

Fig. 12 Predicted limiting grouting pressures

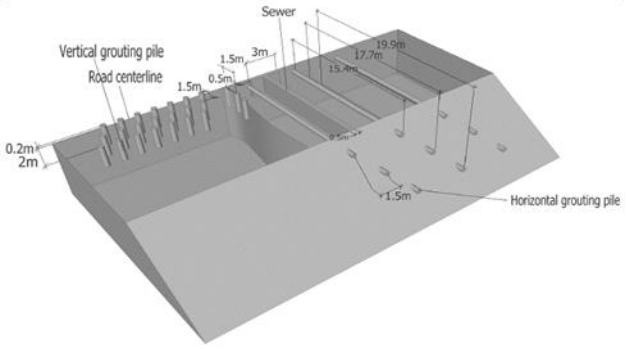

Fig. 13 General arrangement of grouting pipes and sewer

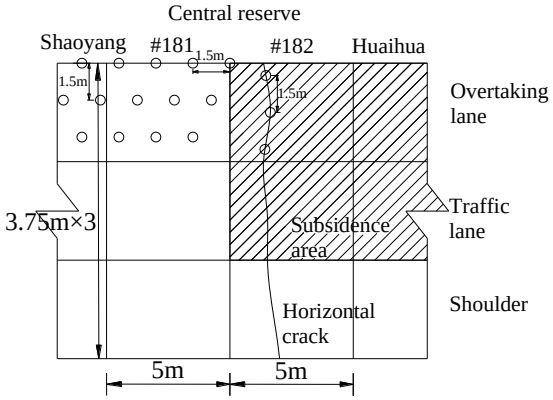

Fig. 14 Plane arrangement of vertical grouting pile

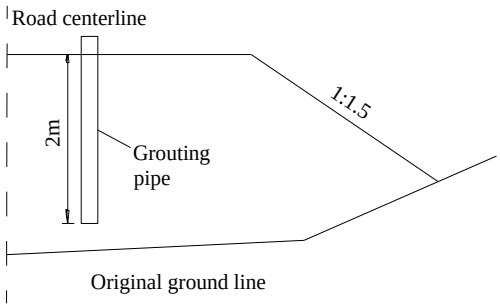

Fig. 15 Profile arrangement of vertical grouting pile

the upper filled soil mass were effected by the infiltration of rain water along pavement crack, which resulted in the

aggravated settlement of the subgrade. The comfort and safety of driving had been greatly reduced. Therefore, it is necessary to reinforce the subgrade.

The settlement area of Shao-huai K1302 highway lies in the traffic lanes and overtaking lanes, across #180~#185 six cement panels. Among these cement panels, the settlement of #183 panel on overtaking lane was most serious. #182 panel, located at the junction of filling and digging, had produced a transverse crack through half of the subgrade, as shown in Fig.11.

6.2 Grouting design

Based on the geological exploration, compaction grouting was chosen to reinforce the subgrade and improve the bearing capacity. The grouting design parameters such as the limiting grouting pressure, grout hole spacing and grouting depth were determined by the proposed model.

Meanwhile, a uniform control standard of grouting is adopted to ensure that the grouting form is compaction grouting rather than fracture grouting. In the grouting process, the grouting quantity in a single hole, the grouting pressure and the lifting displacement are used as the control standards for stopping grouting, respectively. The specific standards are as follows:

①When the single hole grouting quantity does not meet the design standard, but the grouting pressure has reached the design final pressure and the time is maintained for more than 5 minutes, the grouting should be stopped;

②When the grouting pressure does not reach the design final pressure, but the single hole grouting quantity has reached the design standard and the grouting pressure can reach the design final pressure by adjusting the gelling time of the slurry, the grouting should be stopped;

Fig. 16 Site construction drawing of vertical pile grouting

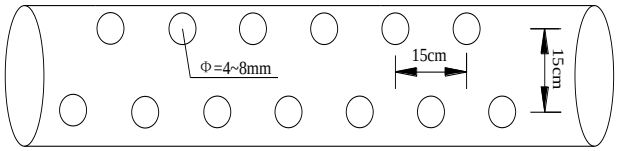

Fig. 17 Schematic diagram of grouting hole on vertical pipe

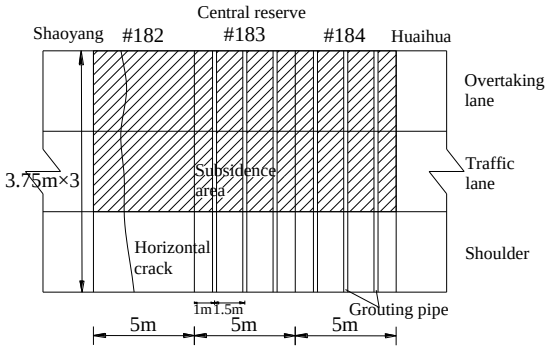

Fig. 18 Plane arrangement of horizontal grouting pile

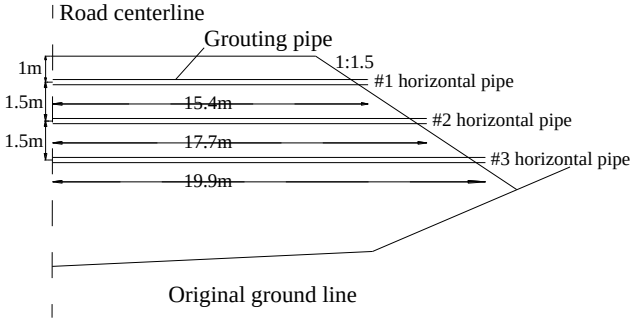

Fig. 19 Profile arrangement of horizontal grouting pile

③If the subgrade lifting displacement exceeds the allowable value, the grouting should be stopped immediately. Grouting quantity, grouting pressure and lifting displacement could be as the control standard for terminated grouting as long as one of the three is satisfied design value.

The soil parameters were adopted from Table 2 for R_l=0.025m and n=0.5, and the results are shown in Fig.12. When the grouting depth was chosen 2 m, the limiting grouting pressure p_{lim} was 1.14 MPa, the grout bulb radius was 0.21 m, and the grout hole spacing was obtained as 1.45 m. The grouting reinforcement schemes, combining the vertical pile grouting and horizontal pile grouting and setting the sewer, were designed to deal with this subgrade settlement, as shown in Fig. 13.

Fig. 20 Site construction drawing of horizontal pile grouting

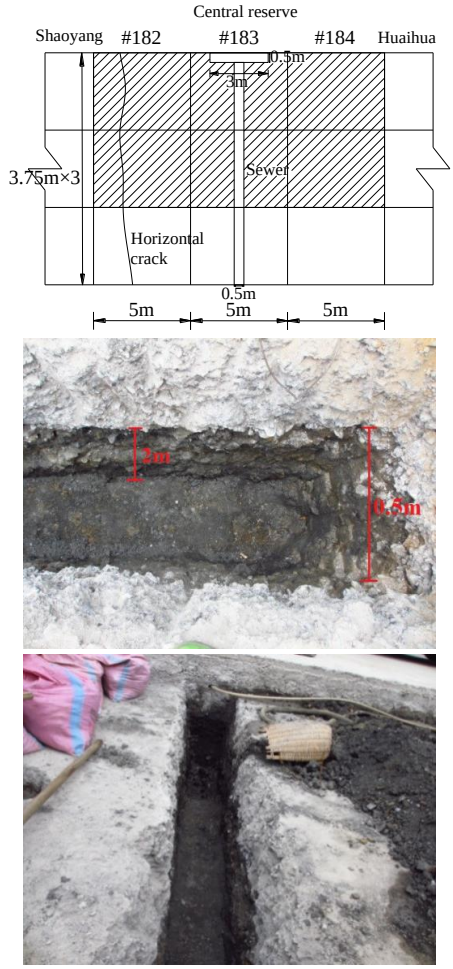

Fig. 21 Plane arrangement of sewer

6.2.1 Vertical pile grouting

The vertical pipe grouting was carried out by digging out the surface of #180~#182 cement panels and using a small drill to drill through the water stable base. The grouting hole spacing was 1.5 m, the grouting depth was 2 m and the grouting pressure was 1.2 MPa, as shown in Figs.14-15. For the cracking of subgrade, the grouting hole was added along the crack and the spacing was 1.5 m. Additionally, grouting pipe was set to be 15~20 cm higher than water stable base.

The scaffolding steel pipe with diameter of 50 mm and wall thickness of 3 mm was used as the vertical grouting pipe. Some grouting holes with a diameter of 4~8 mm was drilled every 15 cm and arranged in a plum shape.

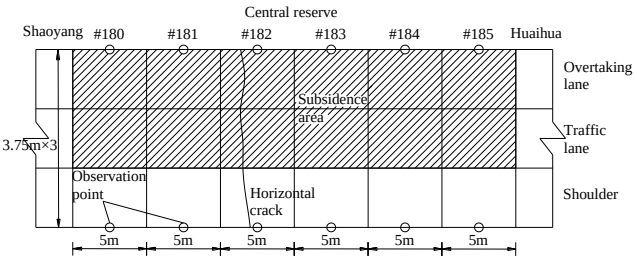

Fig. 22 Plane arrangement of single point settlement gauge

Fig. 23 Upheave of the ground surface

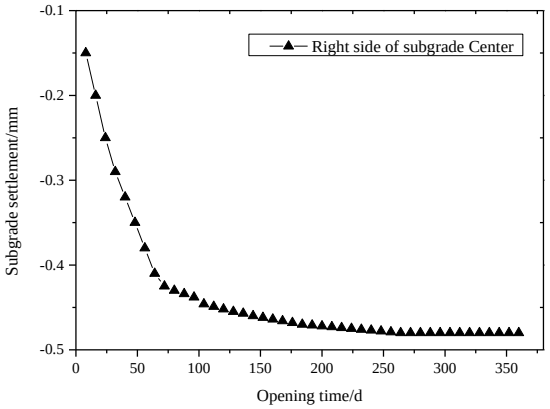

Fig. 24 The settlement of the right-side subgrade after grouting

6.2.2 Horizontal pipe grouting

To improve the grouting effect, the horizontal pipe grouting was carried out on #183~#185 cement panels (Fig.18). The horizontal pipes were inserted into subgrade from the slope edge to road centerline, along the direction perpendicular to driving. The construction of horizontal pipe grouting was divided into three layers, which were 1

m, 2.5 m and 4 m away from the subgrade surface respectively. The length of the corresponding grouting pipes were 1 m,2 m and 3 m respectively, and the horizontal spacing was 1.5 m. Meanwhile, the pipes were set to be 20 cm longer than the slope edge, as shown in Fig. 19. The grouting pressure was adopted 1.2 MPa. The scaffolding steel pipe were also adopted as horizontal grouting pipe and the layout of the grouting hole were the same as vertical grouting pipe. The only difference was that the bottom of the scaffolding pile is reserved for 20 cm long without drilling.

6.2.3 Setting the sewer

The sewer was designed as a rectangular with depth 2 m and width 0.5 m, which is shown in Fig. 21. The water in subgrade work area was collected in the trench and drained to the slope outer edge along the ditch. The larger pebbles were filled in the bottom and middle of ditch, whose both sides and the upper part were layered by a certain percentage (layer thickness is about 15 cm).

6.3 Grouting reinforcement effectiveness

To verify the effectiveness of the grouting reinforcement schemes, the settlement of the right-side subgrade was measured by single point settlement gauge, which was arranged at the center of the panel, as shown in Fig.22.

The settlement curve of the right-side subgrade after grouting is shown in Fig.24, and the upheaval of the ground surface is shown in Fig. 23

It can be seen from Fig. 24 that the settlement of the right-side subgrade is about 0.5 cm in one year and becoming stability, which can meet the requirements of the soft soil subgrade for post-construction settlement and tends to be stable after one year. The properties of the soil and the stability of the subgrade have been improved after grouting.

7. Conclusions

Based on the theory of cavity expansion and the three-dimensional conical shear failure above the grout bulb, an improved prediction model for the limiting grouting pressure of compaction grouting was proposed in this study. The validity and accuracy of the proposed model were verified by compared with EI-Kelesh's solution (2001) and numerical method results. Furthermore, the proposed model was used to guide the design of the subgrade settlement treatment of Shao-huai highway, determining the grouting design parameters such as the limiting grouting pressure, grout hole spacing and grouting depth. The grouting reinforcement schemes were designed, combining the vertical pile grouting and horizontal pile grouting and setting the sewer. Meanwhile, the numerical analysis of the grouting effect shows that the above schemes can achieve the expected goal and the proposed model has a certain reference value for the subgrade settlement treatment of highways.

However, more work should be conducted to confirm the model at specific conditions, develop the at-failure model to govern the cohesive-frictional soils and verify different parameter of failure surface shape *n*.

Acknowledgments

This work was supported by Guizhou Provincial Science and Technology Major Project, No. Qian-ke-he-zhong-da-zhuan-xiang-zi [2018]3010.

References

Brown, D.R. and Warner, J. (1973), "Compaction grouting", *J. Soil Mech. Found. Div.*, **99**(8), 589-601.

Carter, J.P., Booker, J.R. and Yeung, S.K. (1986), "Cavity expansion in cohesive frictional soils", *Géotechnique*, **36**(3), 349-358.

Carter, J.P., Randolph, M.F and Wroth, C.P. (2010), "Stress and pore pressure changes in clay during and after the expansion of a cylindrical cavity", *Int. J. Numer. Anal. Meth. Geomech.*, **3**(4), 305-322. https://doi.org/10.1002/nag.1610030402.

Chai, J.C., Hossain, M.J., Carter, J. and Shen, S.L. (2014), "Cone penetration-induced pore pressure distribution and dissipation", *Comput. Geotech.*, **57**(4), 105-113. https://doi.org/10.1016/j.compgeo.2014.01.008.

Chen, G.H., Zou, J.F. and Qian, Z.H. (2019a), "An improved collapse analysis mechanism for the face stability of shield tunnel in layered soils", *Geomech. Eng.*, **17**(1), 97-107. https://doi.org/10.12989/gae.2019.17.1.097.

Chen, G.H., Zou, J.F., Min, Q., Guo, W.J. and Zhang, T.Z. (2019b), "Face stability analysis of a shallow square tunnel in non-homogeneous soils", *Comput. Geotech.*, **114**, 103112. https://doi.org/10.1016/j.compgeo.2019.103112.

Chen, G.H., Zou, J.F. and Chen, J.Q. (2019c), "Shallow tunnel face stability considering pore water pressure in non-homogeneous and anisotropic soils", *Comput. Geotech.*, **116**, 103205. https://doi.org/10.1016/j.compgeo.2019.103205.

Chen, R.P., Tang, L.J., Yin, X.S., Chen, Y.M. and Bian, X.C. (2015), "An improved 3D wedge-prism model for the face stability analysis of the shield tunnel in cohesionless soils", *Acta Geotech.*, **10**(5), 683-692. https://doi.org/10.1007/s11440-014-0304-5.

D'Antonio, R.G., Lay, G., Wan, J., Su, N., Cruz, O. and Shao, L. (2014), "Admiralty way ground improvement case study", *Proceedings of the Geo-Congress 2014*, Atlanta, Georgia, U.S.A., February.

El-Kelesh, A.M., Mossaad, M.E. and Basha, I.M. (2001), "Model of compaction grouting", *J. Geotech. Geoenviron. Eng.*, **127**(11), 955-964. https://doi.org/10.1061/(ASCE)1090-0241(2001)127:11(955).

El-Kelesh, A.M., Matsui, T. and Tokida, K.I. (2012), "Field investigation into effectiveness of compaction grouting", *J. Geotech. Geoenviron. Eng.*, **138**(4), 451-460. https://doi.org/10.1061/(ASCE)GT.1943-5606.0000540.

Fahimifar, A., Ghadami, H. and Ahmadvand, M. (2015), "The ground response curve of underwater tunnels, excavated in a strain-softening rock mass", *Geomech. Eng.*, **8**(3), 323-359. http://dx.doi.org/10.12989/gae.2015.8.3.323.

Fischer, J.A., Mcwhorter, J.G. and Fischer, J.J. (2012), "Geological and geotechnical aspects of grouting in karst", *Proceedings of the 4th International Conference on Grouting and Deep Mixing*, New Orleans, Louisiana, U.S.A., February.

Graf, E.D. (1969), "Compaction grouting technique and observations", *J. Soil Mech. Found. Div.*, **95**(5), 1151-1158.

Hossain, M.A. and Yin, J.H. (2014), "Behavior of a pressure-grouted soil-cement interface in direct shear tests", *Int. J. Geomech.*, **14**(1), 101-109. https://doi.org/10.1061/(ASCE)GM.1943-5622.0000301.

Ibrahim, E., Soubra, A.H. and Mollon, G. (2015), "Three-dimensional face stability analysis of pressurized tunnels driven

in a multilayered purely frictional medium", *Tunn. Undergr. Sp. Technol.*, **49**(01),18-34. https://doi.org/10.1016/j.tust.2015.04.001.

Li, C., Zou, J.F. and A, S.G. (2019), "Closed-form solution for undrained cavity expansion in anisotropic soil mass based on spatially mobilized plane failure criterion", *Int. J. Geomech.*, **19**(7), 04019075. https://doi.org/10.1061/(ASCE)GM.1943-5622.0001458.

Pan, Q. and Dias, D. (2017), "Upper-bound analysis on the face stability of a non-circular tunnel", *Tunn. Undergr. Sp. Technol.*, **62**, 96-102. https://doi.org/10.1016/j.tust.2016.11.010.

Pan, Q. and Dias, D. (2018), "Three dimensional face stability of a tunnel in weak rock masses subjected to seepage forces", *Tunn. Undergr. Sp. Technol.*, **71**, 555-566. https://doi.org/10.1016/j.tust.2017.11.003

Pegues, J.C., Jordan, J.A. and Xu, Y. (2015), "Ground improvement: Difficulties in measuring success", *Proceedings of the International Foundations Congress and Equipment Expo 2015*, San Antonio, Texas, U.S.A., March.

Szynakiewicz, T. (2016), "Compaction grouting for ground improvement and structure rehabilitation", *Proceedings of the Biennial Rocky Mountain Geo-Conference*, Golden, Colorado, U.S.A., November.

Taylor, R.M. and Choquet, P. (2014), "Automatic monitoring of grouting performance parameters", *Proceedings of the International Conference on Grouting and Deep Mixing*, New Orleans, Louisiana, U.S.A., February.

Ukritchon, B., Yingchaloenkitkhajorn, K. and Keawsawasvong, S. (2017), "Three-dimensional undrained tunnel face stability in clay with a linearly increasing shear strength with depth", *Comput. Geotech.*, **88**, 146-151. https://doi.org/10.1016/j.compgeo.2017.03.013.

Vesic, A.S. (1972), "Expansion of cavities in infinite soil mass", *J. Soil Mech. Found. Div.*, **98**(3), 265-269.

Wong, H.Y. (1971), *Compaction of Soil during Pressure Grouting*, Private Rep., Cementation Research Ltd., Rickmansworth, Herts, England.

Wong, H.Y. (1974), "Discussion of compaction grouting", *J. Geotech. Eng. Div.*, **100**(5), 556-559.

Warner, J. and Brown, D.R. (1973), "Planning and performing compaction grouting", *J. Geotech. Eng. Div.*, **100**(6), 653-666.

Wang, S.L., Yin, S.D. and Wu, Z.J. (2012), "Strain-softening analysis of a spherical cavity", *Int. J. Numer. Anal. Meth. Geomech.*, **36**(2), 182-202. https://doi.org/10.1002/nag.1002.

Wang, S.Y., Chan, D.H., Lam, K.C. and Au, S.K.A. (2010), "Effect of lateral earth pressure coefficient on pressure controlled compaction grouting in triaxial condition", *Soils Found.*, **50**(3), 441-445. https://doi.org/10.3208/sandf.50.441.

Wang, S.Y., Chan, D.H., Lam, K.C. and Au, S.K.A. (2013), "A new laboratory apparatus for studying dynamic compaction grouting into granular soils", *Soils Found.*, **53**(3), 462-468. https://doi.org/10.1016/j.sandf.2013.04.007.

Xiao, Y., Liu, H., Chen, Y., Jiang, J. and Zhang, W. (2015), "State-dependent constitutive model for rockfill materials", *Int. J. Geomech.*, **15**(5), 04014075. https://doi.org/10.1061/(ASCE)GM.1943-5622.0000421.

Xiao, Y. and Liu, H. (2017), "Elastoplastic constitutive model for rockfill materials considering particle breakage", *Int. J. Geomech.*, **17**(1), 04016041. https://doi.org/10.1061/(ASCE)GM.1943-5622.0000681.

Yang, X.L. and Pan, Q.J. (2015), "Three dimensional seismic and static stability of rock slopes", *Geomech. Eng.*, **8**(1), 97-111. http://dx.doi.org/10.12989/gae.2015.8.1.097.

Yang, X.L. and Yan, R.M. (2015), "Collapse mechanism for deep tunnel subjected to seepage force in layered soils", *Geomech. Eng.*, **8**(5), 741-756. https://doi.org/10.12989/gae.2015.8.5.741.

Yea, G.G., Kim, T.H., Kim, J.H. and Kim, H.Y. (2013), "Rehabilitation of the core zone of an earth-fill dam", *J. Perform. Construct. Facil.*, **27**(4), 485-495. https://doi.org/10.1061/(ASCE)CF.1943-5509.0000335.

Zhang, C., Han, K. and Zhang, D. (2015), "Face stability analysis of shallow circular tunnels in cohesive–frictional soils", *Tunn. Undergr. Sp. Technol.*, **50**, 345-357. https://doi.org/10.1016/j.tust.2015.08.007.

Zhou, H., Kong, G., Li, P. and Liu, H. (2015), "Flat cavity expansion: theoretical model and application to the interpretation of the flat dilatometer test", *J. Eng. Mech.*, **212**(1), 1-7. https://doi.org/10.1061/(ASCE)EM.1943-7889.0000957.

Zhou, H., Kong, G. and Liu, H. (2016), "A semi-analytical solution for cylindrical cavity expansion in elastic–perfectly plastic soil under biaxial in situ stress field", *Géotechnique*, **66**(7), 1-12. http://dx.doi.org/10.1680/jgeot.15.P.115.

Zou, J.F. and Xia, M.Y. (2016), "Uplift capacity of shallow anchors based on the generalized nonlinear failure criterion", *Math. Prob. Eng.*, 1-9. http://dx.doi.org/10.1155/2016/3082047.

Zou, J.F., Xia, Z.Q. and Dan, H.C. (2016), "Theoretical solutions for displacement and stress of a circular opening reinforced by grouted rockbolt", *Geomech. Eng.*, **11**(3), 439-455. https://doi.org/10.12989/gae.2016.11.3.439.

Zou, J.F. and Xia, M.Y. (2017), "A new approach for the cylindrical cavity expansion problem incorporating deformation dependent of intermediate principal stress", *Geomech. Eng.*, **12**(3), 347-360. https://doi.org/10.12989/gae.2017.12.3.347.

Zou, J.F. and Wei, X.X. (2018), "An improved radius-incremental-approach of stress and displacement for strain-softening surrounding rock considering hydraulic-mechanical coupling", *Geomech. Eng.*, **16**(1), 59-69. https://doi.org/10.12989/gae.2018.16.1.059.

Zou, J.F., Wei, A. and Yang, T. (2018), "Elasto-plastic solution for shallow tunnel in semi-infinite space", *Appl. Math. Modell.*, **64**(12), 669-687. https://doi.org/10.1016/j.apm.2018.07.049.

Zou, J. F., Yang, T., Ling, W., Guo, W. and Huang, F. (2019a), "A numerical stepwise approach for cavity expansion problem in strain-softening rock or soil mass", *Geomech. Eng.*, **18**(3), 225-234. https://doi.org/10.12989/gae.2019.18.3.225.

Zou, J.F., Chen, G.H. and Qian, Z.H. (2019b), "Tunnel face stability in cohesion-frictional soils considering the soil arching effect by improved failure models", *Comput. Geotech.*, **106**(2), 1-17. https://doi.org/10.1016/j.compgeo.2018.10.014.

Zou, J.F., Liu, S.X., Li, J.B. and Qian, Z.H. (2019c), "Face stability analysis for a shield-driven tunnel with non-linear yield criterion", *Proc. Inst. Civ. Eng. Geotech. Eng.*, **172**(3), 243-254. https://doi.org/10.1680/jgeen.17.00222.

Zou, J.F. and Zhang, P.H. (2019), "Analytical model of fully grouted bolts in pull-out tests and in situ rock masses", *Int. J. Rock Mech. Min. Sci.*, **113**(1), 278-294. https://doi.org/10.1016/j.ijrmms.2018.11.015.

CC